Miniature Quad-rotor Dynamics Modeling & Guidance for Vision-based Target Tracking Control Tasks

A. Barrientos, and J. Colorado, *Members, IEEE*

Abstract— **This paper presents the dynamics modeling and the control & guidance architecture for specific target tracking indoors tasks using a miniature quad-rotor. Our objective is to develop a testbed using Matlab for experimentation and simulation of dynamics, control and guidance methods within a strong interplay between the hardware on board and software provisioned.**

I. INTRODUCTION

Recent progress in MEMS [1] sensor technology, data processing, and integrated actuators has made the development of miniature flying robots fully possible. Depending on the flying principle and the propulsion mode, those Micro or mini Aerial Vehicles-MAV can be classified into multiple categories: fixed, flapping, morphing and rotary wings are the most common mechanisms developed [2]. As usual, those mechanisms have a wingspan or rotor span less than 15cm with a total weight less than 100 grams, and generally equipped with MEMS sensors (gyros, accelerometers) and miniature cameras.

Depending of the size of the MAV, researches focus on different phenomena and new paradigms and challenges related to mechanical design, biological-inspired locomotion [3], [4], [5] and new approaches for gaining more level of autonomy (see Fig. 1 for a sneak peek at the MAV's state-of-the-art).

In this sense, the aim of this work is to present a complete testbed for miniature four rotor-wing aerial vehicles, which allows the testing of dynamics models, guidance, control strategies and hardware description (sensors on board) for making those mechanism even more autonomous.

The testbed purpose is for prototype design matters or being used as a control mainframe station. For simulation results validation, we have constraint the experiment for target tracking tasks that require vision sensing for that purpose (the testbed can adopt other scenarios).

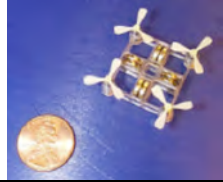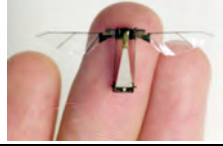|	
	NanoFlyer **Proxflyer Company** -Rotor: 60 mm diameter -Weight: 3.3 grams -Flight time: Up to 1 minute -Tele-operated system.
	Mini Flying Robot **EPSON Corporation** - 12.3 g helicopter - Diameter: About 136 mm - Height: About 85 mm - Flight time: About 3 minutes
	Mesicopter **Stanford University** - 4 motor design - 1.5 cm rotor diameters - Weight of the 325mg
	Harvard University - 60-milligrams - Piezoelectric actuator
	MFI **Berkeley University** - 2 wing carbon fiber - 25mm (wingtip to wingtip) flapping wing micro

Fig. 1 MAV sneak peek at the state-of-the-art

II. MICRO QUAD-ROTOR MODELING

This section presents some morphological characteristics of the mini quad-rotor system, going from the kinematics frames to the 6-DoF dynamics equation of motion.

A. Kinematics Frames of Reference.

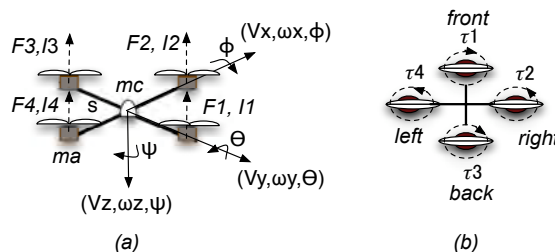The quadrotor is an underactuated mechanical system with 6-DoF and only four actuators.

Fig. 2 (a) quad-rotor motion variables. (b) quad-rotor sense of motion.

The main forces and moments acting on it are those produced by the propellers. Those four propellers are in cross configuration, meaning that the two pair or propellers (1,3) and (2,4) showed in Fig.2-b, turn in opposite directions. By modifying the rotor speed, the lift force changes in order to generate motion. The rotation of a rigid body in space can be parameterized using several methods: Euler angles, quaternion, Tait-Bryan angles, etc. [6]. However, the most extensively used method in aerospace engineering is the Euler angles. Those angles, as well as the quad-rotor and inertial frames are shown in Fig. 3.
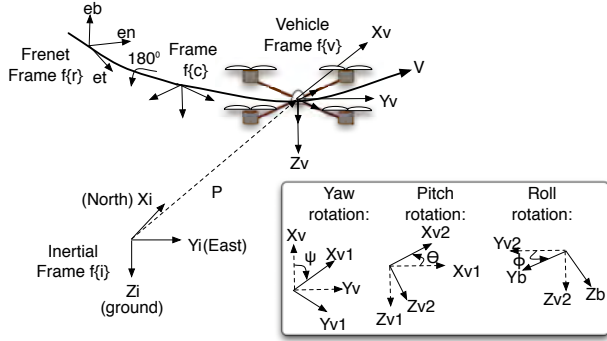

Fig. 3 Kinematics frames.

The inertial frame f{i} is a ground fixed coordinate system and the vehicle frame f{v} is located at the center of mass of the quad-rotor. The complete rotation matrix, called Direct Cosine Matrix [7], consists in rotating a 'ϕ' roll angle about *x-axis,* a 'θ' pitch angle about *y-axis,* and a 'ψ' yaw angle about *z-axis,* then:

$$R(\phi,\theta,\psi) = R_z(\psi)R_y(\theta)R_x(\phi)$$

$$R(\phi,\theta,\psi) = \begin{bmatrix} c\psi c\theta & c\psi s\theta s\phi - s\psi c\phi & c\psi s\theta c\phi + s\psi s\phi \\ s\psi c\theta & s\psi s\theta s\phi + c\psi c\phi & s\psi s\theta c\phi - s\phi c\psi \\ -s\theta & c\theta s\phi & c\theta c\phi \end{bmatrix} \quad (1)$$

In addition, to obtain the time variation of the Euler angles $(\dot{\phi},\dot{\theta},\dot{\psi})$ is necessary to relate the body angular rates measured with the gyroscope (p,q,r).

Since $(\dot{\phi},\dot{\theta},\dot{\psi})$ rates are small values, and noting that: $R_x(\dot{\phi}) = R_y(\dot{\theta}) = R_z(\dot{\psi}) = U$, being U the identity operator, this relation is:

$$\begin{bmatrix} p \\ q \\ r \end{bmatrix} = R_x(\dot{\phi})\begin{bmatrix} \dot{\phi} \\ 0 \\ 0 \end{bmatrix} + R_x(\phi)R_y(\dot{\theta})\begin{bmatrix} 0 \\ \dot{\theta} \\ 0 \end{bmatrix} + R_x(\phi)R_y(\theta)R_z(\dot{\psi})\begin{bmatrix} 0 \\ 0 \\ \dot{\psi} \end{bmatrix} \quad (2)$$

B. Single Rigid Body Dynamics

For defining the dynamics equation of motion, the mini quad-rotor is regarded as a single rigid body system with 6-DoF. This body is free to move under the actions of the

gravity, gyroscopic, moments, and aerodynamic forces. Likewise, we use the Newton-Euler formalism to define the dynamics of the rigid body under external forces applied to the center of mass expressed in the vehicle frame f{v}, as:
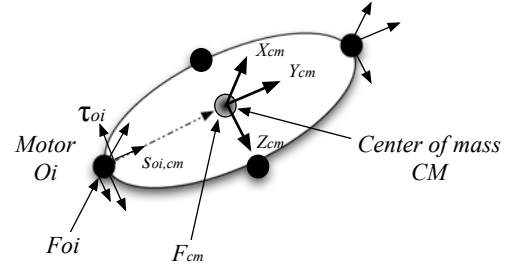

Fig. 4 Rigid body diagram.

Assuming from Fig. 4 that O_i and *CM* are two points located on the rigid body, which corresponds to the location of a motor propeller and the center of mass of the vehicle respectively, the $s_{oi,cm} \in \Re^3$ vector relate both points. Likewise, the translational and angular velocities (*v, w*) and forces (*f,* τ) respectively at any point on a body in $\Re^3$ are related as:

$$\begin{aligned} w_{cm} &= w_{oi} \\ v_{cm} &= v_{oi} + w_{oi} \times s_{oi,cm} \\ f_{cm} &= f_{oi} \\ \tau_{cm} &= \tau_{oi} + f_{oi} \times s_{oi,cm} \end{aligned} \quad (3)$$

In terms of spatial algebra [8], the physical quantities from (3) are represented as a 6x1 column vectors, and each incorporates the appropriate angular and translational components stacked together. Those terms now in $\Re^6$ with respect to the CM of the body are:

$$V_{cm} = \begin{bmatrix} \omega_{cm} \\ v_{cm} \end{bmatrix}, \quad \dot{V}_{cm} = \begin{bmatrix} \dot{\omega}_{cm} \\ \dot{v}_{cm} \end{bmatrix}, \quad F_{cm} = \begin{bmatrix} \tau_{cm} \\ f_{cm} \end{bmatrix} \quad (4)$$

Using this spatial notation, the acceleration in $\Re^6$ is:

$$\begin{aligned} \dot{V}_{cm} &= S_{oi,cm}^T \dot{V}_{oi} + \dot{S}_{oi,cm}^T V_{oi} \\ \dot{V}_{cm} &= S_{oi,cm}^T \left[S_{oi,cm} I_{cm}^{-1} S_{oi,cm}^T F_{oi} \right] + \dot{S}_{oi,cm}^T V_{oi} \end{aligned} \quad (5)$$

Where $S_{oi,cm} \in \Re^{6x6}$ is the operator for relating translations from O_i to CM's point. The term $I_{cm} \in \Re^{6x6}$ is the mass operator, and $\dot{S}_{oi,cm}^T V_{oi}$ represents both coriolis and centrifugal acceleration terms.

C. Quad-rotor dynamics.

First of all, we define forces based on inertial effects and then we address aerodynamics and motor effects. In

addition, the $F_{oi} \in \Re^6$ term is composed by both thrust and drag moment, which are proportional to the square of the propeller rotation speed ω. Finally, by using the kinematics transformations previously defined, and representing high-level notation dynamics from (5) into low-level state-equations:

$$\ddot{P}_x = F_{cm,x} \frac{c\phi s\theta c\psi + s\phi s\psi}{m} \quad \ddot{\phi} = \frac{J_{cm,y} - J_{cm,z}}{J_{cm,x}} \dot{\theta}\dot{\psi} + J_{cm,x}^{-1} \tau_{cm,x}$$

$$\ddot{P}_y = F_{cm,y} \frac{c\phi s\theta s\psi - s\phi c\psi}{m} \quad \ddot{\theta} = \frac{J_{cm,y} - J_{cm,z}}{J_{cm,x}} \dot{\phi}\dot{\psi} + J_{cm,y}^{-1} \tau_{cm,y} \quad (6)$$

$$\ddot{P}_z = F_{cm,z} \frac{c\phi c\theta - g}{m} \quad \ddot{\psi} = \frac{J_{cm,x} - J_{cm,y}}{J_{cm,z}} \dot{\phi}\dot{\theta} + J_{cm,z}^{-1} \tau_{cm,z}$$

The rolling torque is produced by the forces of the right and left motors: τ_2 and τ_4 respectively (see Fig. 2b) and similarly, the pitching torque is produced by the forces of the front and back actuators: τ_3 and τ_1.

III. SENSORS ON BOARD

A. Camera modeling

The camera model (shown in Fig. 5) is used for tracking the target on ground in order to control altitude and forward/backward motion. The position of the target is given by the vector $P_{[xyz]}$, which corresponds to the pixel location on image plane: $(\varepsilon_x, \varepsilon_y)$. The objective is to project the target position onto the frame of reference of the camera. These relationship is obtained by relating the camera field-of-view (FoV): η, the height above ground $-P_z$, the lateral position error P_y, the roll angle ϕ, and the total number of pixels along the lateral axis of the camera: M_x and M_y.
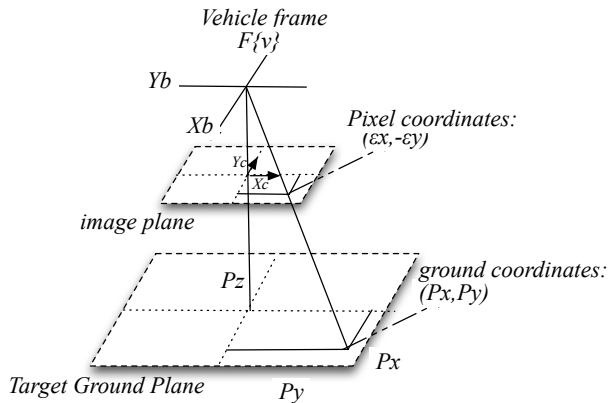

Fig. 5 Camera model for ground target tracking.

This target/image plane relation is:

$$P_x = -P_z \tan\left(\theta - \varepsilon_y \frac{\eta}{M_y}\right), \quad P_y = -P_z \tan\left(\phi - \varepsilon_x \frac{\eta}{M_x}\right) \quad (7)$$

B. MEMS Gyro and Accelerometers

The most commonly used MEMS gyroscopes are the hemispherical resonant type [9], also known as wine glass gyro, in which a current passing through the conducting legs creates a force that resonates the ring. Induced voltages detect this Coriolis-induced ring motion as the legs cut the magnetic field. Simple equation can be used to describe how the Coriolis effect changes the frequency of the vibration, thus detecting the rotation. Likewise, the most successful accelerometer types are based on capacitive transduction; the reasons are the simplicity of the sensor element itself. Those ones contain a small plate attached to torsion levers. The plate rotates under acceleration and changes the capacitance between the plate and the surrounding walls. Both analog output of gyros and accelerometers are given by:

$$v_{gyro} = k_{gyro}\omega + \beta_{gyro} + \eta_{gyro}$$
$$v_{accel} = k_{accel}A + \beta_{accel} + \eta_{accel} \quad (8)$$

The v term is the output of the gyro/accel (volts), k is a gain constant, β is the bias term strongly dependent on temperature, and finally the η is the zero mean white noise.

IV. ARCHITECTURE FOR CONTROL & GUIDANCE

As shown in Fig 7, three main modules compose the quad-rotor Matlab testbed architecture: *The vehicle model*: which incorporates the dynamics equations, camera model, sensors and filtering stage. *The control Module* and the *estimation Module,* which uses the Kalman filtering theory [10] for state observation, and the Frenet Serret theory [11] as a complement for setting accuracy attitude references.

A. Kalman Filtering and Frenet Serret Formulas

The Extended Kalman Filter –EKF is basically composed by four stages named as: *Prediction, Observation, Comparison, and Correction,* as depicted in Fig. 6.
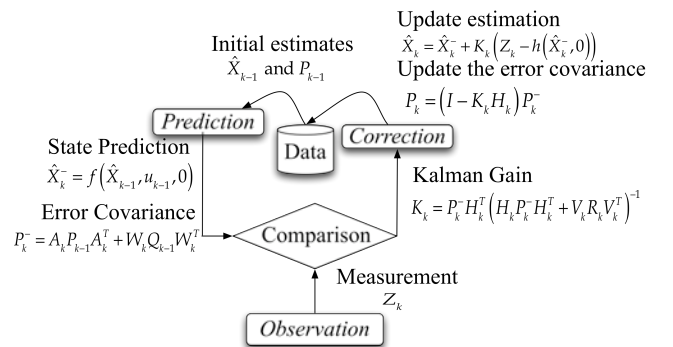

Fig. 6 Extended Kalman filter for state estimation.

The rate gyros and accelerometers will be used to drive the <u>Prediction</u> stage, and the camera and an optic sensor (to
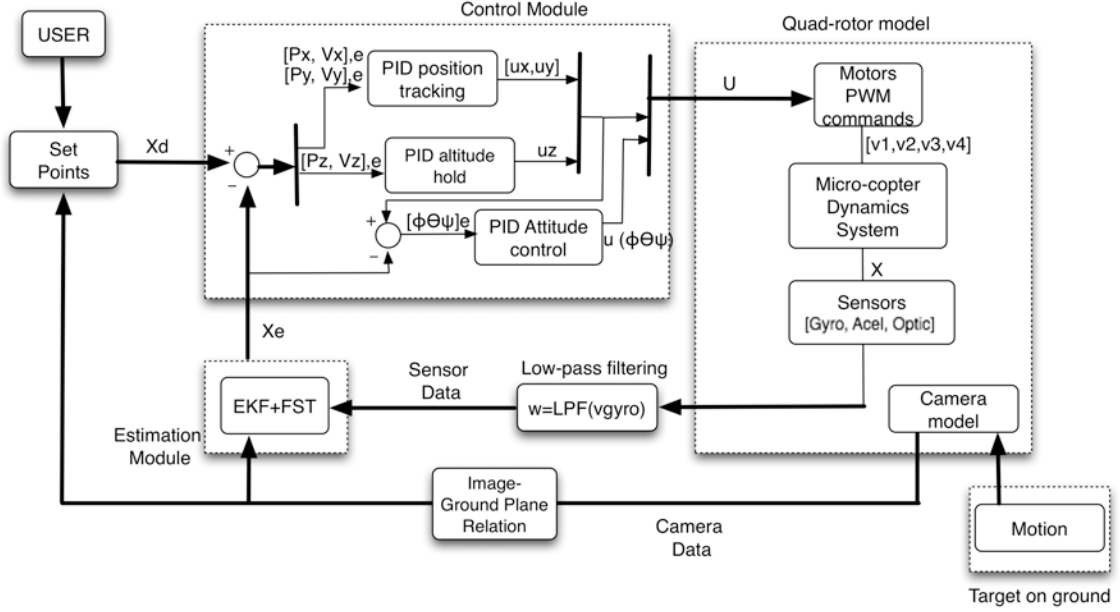
Fig. 7 Testbed architecture for Miniature Quad-rotor guidance & Control.

measure altitude) will be used in the <u>Correction</u> stage. The propagation model $f(\hat{X},U)$ is defined from the partial derivatives of the non-linear model from (8). Using the EKF, we also estimate the attitude of the vehicle. However, when the target on ground performs aggressive changes in orientation and speed motion, the estimation of the roll, pitch and yaw angles of the vehicle is not enough reliable. To solve this issue, we introduce the use of the Serret-Frenet formulas, allowing the estimation of the attitude as a function of the speed and acceleration of the vehicle. From Fig. 3, *the Frenet frame - f{r} and the rotated Frenet frame - f{c},* (both useful for the definition of the Euler angles) are shown. In vector calculus the Frenet–Serret formulas describe the kinematic properties of a particle that moves along a continuous, differentiable curve in three-dimensional Euclidian space $\Re^3$. More specifically, the formulas describe the derivatives of the so-called tangent (e_t), normal (e_n), and binormal (e_b) unit vectors in terms of each other (see Fig 3). The position and magnitude of the velocity vector at any point of the trajectory are given by:

$$V_p = \left\| \dot{P} \right\| = \sqrt{\dot{P}_x^2 + \dot{P}_y^2 + \dot{P}_z^2} \qquad (9)$$

To every point of the curve we can associate an orthonormal triad of vectors namely the tangent, the normal and the bio-normal (see Fig. 3). The Frenet-Serret theory says that by properly arranging these vectors in a matrix, we obtain a description of the curve orientation due to the position, velocity and acceleration of the vehicle while tracing out the path. The unit vectors are then defined as:

$$e_t = \frac{\dot{P}}{V_p}, \quad e_b = \frac{\dot{P} \times \ddot{P}}{\left\| \dot{P} \times \ddot{P} \right\|}, \quad e_n = e_b \times e_t \qquad (10)$$

According to the notation of rotational transformations used in robotics literature, we can express the coordinates of a vector given in the rotated Frenet-Frame f{c} to the f{i} frame with the matrixes:

$$\begin{aligned}
\beta &= \sin^{-1}\left(\frac{v_y}{\left\|V_p\right\|}\right), \quad \alpha = \tan^{-1}\left(\frac{v_z}{v_x}\right), \\
R_i^c &= R_x(180°)[e_t \quad e_n \quad e_b] \\
R_c^r &= R_y(\alpha)^T R_z(-\beta)^T, \\
R_i^r &= R_c^r R_i^c
\end{aligned} \qquad (11)$$

Where β is the sideslip angle and α the angle of attack. The overall rotation is composed by a rotation about the f{b} *z-axis* through the angle β, followed by a rotation about the f{b} *y-axis* through the angle α, as expressed in (11). Finally, from the transformation R_i^r, the attitude estimation is given by ($r_{i,j}$ refers to its components):

$$\begin{aligned}
\phi &= \text{atan2}(r_{23}, r_{33}), \\
\theta &= \text{atan2}\left(-r_{13}, \sqrt{r_{23}^2 + r_{33}^2}\right), \\
\psi &= \text{atan2}(r_{12}, r_{11})
\end{aligned} \qquad (12)$$

B. The Control Module.

This sub-section introduces the control strategies used to command the Mini quad-rotor while tracking the target on ground. The control design proceeds by developing PID control equations in order to control: *target position tracking, altitude, and attitude (roll, pitch, yaw).* First of all

we describe the control design derived directly after simplifying (6). For control purposes, we assume that both θ and ϕ are small, and the Coriolis effect terms are also negligible, then, we define:

$$\ddot{P}_x = u_x = -c\phi s\theta \frac{F}{m}, \quad \ddot{P}_y = u_y = s\phi \frac{F}{m}, \quad \ddot{P}_z = u_z = g - c\phi c\theta \frac{F}{m} \quad (13)$$

Cartesian position control: u_x, u_y and altitude control: u_z are non-coupled, however, attitude control ($u_{\phi\theta\psi}$) requires the computation of u_x, u_y, u_z. Hence, we develop PID strategies for that. First, we treat altitude hovering based on the size of the target within the camera frame.

Altitude Hovering Control: the control objective is to maintain the vehicle in a constant altitude (P_z) while tracing the trajectory defined by the target on ground. This controller is based on the vision tracking provided by the on-board mini camera, as shown in Fig. 8.
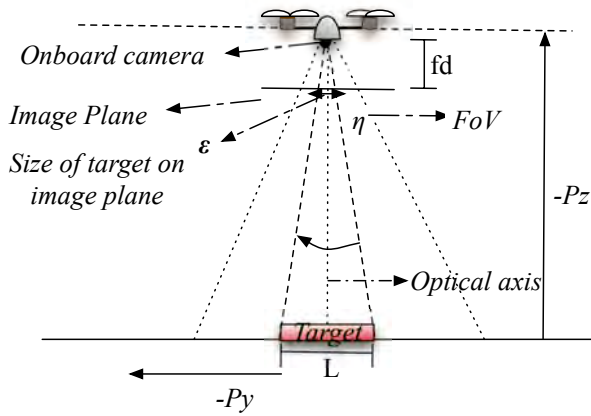

Fig. 8 Front view of the scenario for regulating the Altitude.

The idea is to establish an equation that relates the real size of the target (L), the size of the target projected in the image plane ε (given in pixels), the focal distance fd and the altitude to hold P_z. This equation is easily found using simple triangles relation as:

$$\frac{-P_z}{L} = \frac{f_d}{\varepsilon}$$

$$\ddot{P}_z = u_z = \frac{f_d}{L}\frac{\ddot{\varepsilon}}{\varepsilon^2} - 2f_d L \frac{\dot{\varepsilon}}{\varepsilon^3}, \quad (14)$$

$$\ddot{\varepsilon} = u_z \left(\frac{\varepsilon^2}{f_d L}\right) + 2\frac{\dot{\varepsilon}}{\varepsilon^3}$$

Now, we drive the size of the target ε to the desired one ε^d by using the following PID control equation:

$$PID = K_{p,z}(\varepsilon^d - \varepsilon) - K_{d,z}\dot{\varepsilon} + K_{i,z}\int(\varepsilon^d - \varepsilon)d\tau \quad (15)$$

Equaling terms from (15) and (14), and solving for u_z:

$$u_z = \frac{f_d L}{\varepsilon^2}K_{p,z}(\varepsilon^d - \varepsilon) - \left(\frac{f_d L}{\varepsilon^2}K_{d,z} + 2\frac{f_d L}{\varepsilon}\right)\dot{\varepsilon}$$
$$+ \frac{f_d L}{\varepsilon^2}K_{i,z}\int(\varepsilon^d - \varepsilon)d\tau \quad (16)$$

Attitude Control: As shown in the Testbed architecture from Fig. 7, the attitude set-point commands depends on the ground motion of the target. In order to find the desired force to define those commands, we isolated the *F/m* term from u_z equation in (13), and replace that term within u_x and u_y, then we obtain:

$$\frac{F}{m} = \frac{g - u_z}{c\phi c\theta},$$

$$u_x = s\theta\left(\frac{g - u_z}{c\theta}\right), \quad u_y = s\phi\left(\frac{g - u_z}{c\phi c\theta}\right) \quad (17)$$

Then the desired pitch and roll profile, as a function of target's motion is:

$$\theta^d = \tan^{-1}\left(\frac{u_x}{u_z - g}\right), \quad \phi^d = \tan^{-1}\left(\frac{u_y c\theta}{g - u_z}\right) \quad (18)$$

V. TESTBED SIMULATION RESULTS

For testing the whole architecture within simulation we used Matlab. The conditions of the tracking scenario are:
- The trajectory of the target on ground is known. The velocity of the target is max. 1m/s.
- The constant mini quad-rotor altitude over target is one meter (1m) from ground.
- The mini quad-rotor wingspan is 10cm.
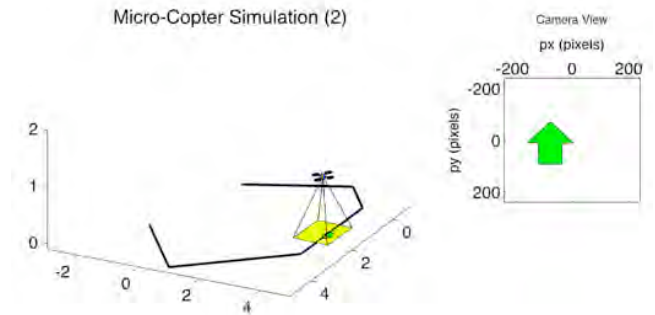- The mini quad-rotor weight is 100 grams.

Fig. 9 Testbed scenario for tracking simulation.

Figure 9 shows the Matlab scenario, where the yellow square represents the field-of-view of the camera, and the green arrow on ground is the target to be tracked. The black line is the given target trajectory, and the right plot of each simulation stage represents how the camera captures the target.
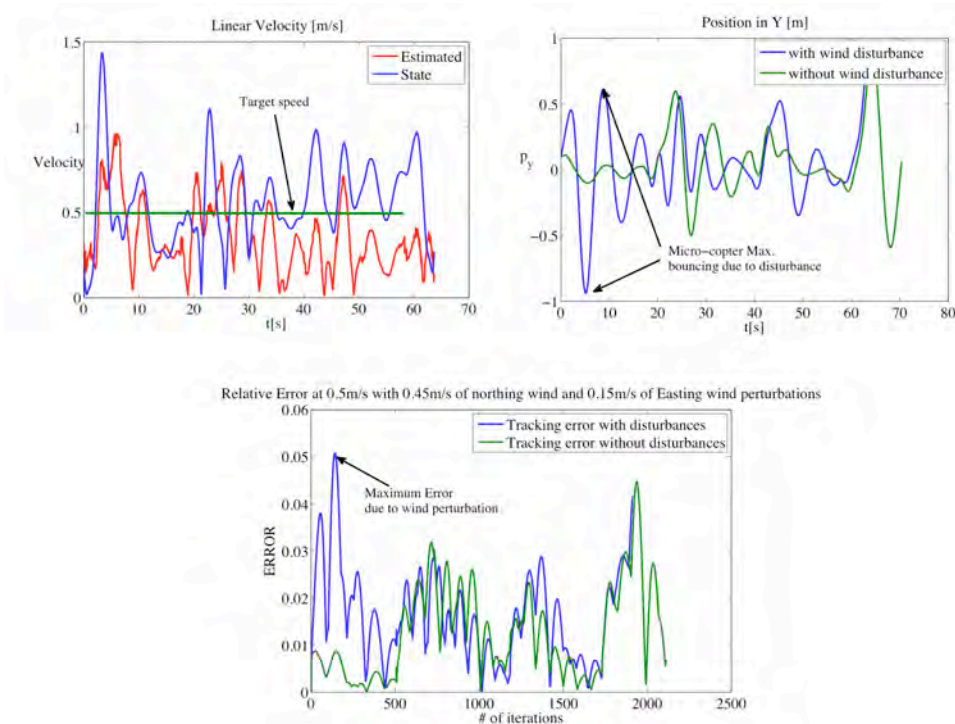
Fig. 10. System response with wind disturbances of 0.45m/s and 0.15m/s in both northing and easting directions.

For simulation results, two test cases are included: 1). The first one consists on verifying if the Micro-copter is capable of tracking the target on ground given a specific trajectory regarding performance based on accurate VS target speed tracking criterion (see Fig. 11). The idea of incorporate the Frenet-Serret formulas within the estimation module, as a complement to the EKF was based on achieving accuracy attitude profile during flight, when the target is performing aggressive orientation changes to approaching speeds up to 1 m/s. 2). In the second test, the control system is capable of fixing wind disturbances up to 0.55m/s in both northing or easting directions (see Fig. 10).
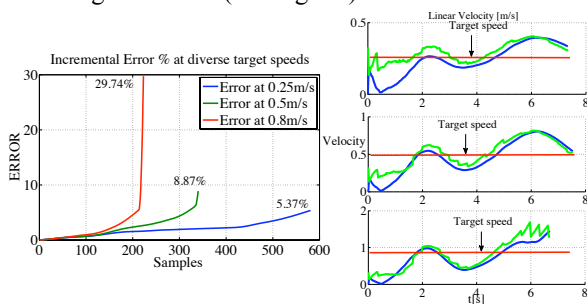

Fig. 11 Incremental Tracking Error percentage at diverse target's speeds

VI. CONCLUSIONS

The Inclusion of the Frenet formulas within the guidance module allowed the MAV improving tracking of the target going from 0.5m/s to 1m/s target speed. This was

achieved due to attitude references were set as a function of the speed and acceleration of the vehicle. On the other hand, the controller module also demonstrates to be robust. Figure 10 shows how the MAV is capable of regulating external air disturbances up to 0.5m/s airspeed.

REFERENCES

[1] T. Pornsin-Shiriak, Y. Tai, H. Nassef, and C. Ho, "Titanium-alloy MEMS wing technology for a micro aerial vehicle application," J. of Sensors and Actuators A: Physical, vol. 89, pp. 95–103, Mar. 2001.

[2] R. Dudley, The Biomechanics of Insect Flight: Form, Function and Evolution. Princeton University Press, 1999.

[3] J. Yan, R. Wood, S. Avadhanula, and M. S. amd R.S. Fearing, "Towards flapping wing control for a micromechanical flying insect," in IEEE Int. Conf. on Robotics and Automation, Seoul, Korea, May 2001.

[4] S.Sunada and C.P. Ellington, "A new method for explaining the generation of aerodynamic forces in flapping flight," Math. Methods Appl. Sci., vol. 24,pp.1377–1386,2001.

[5] T. Mueller and J. DeLaurier, "Aerodynamics of small vehicles," Annu. Rev. Fluid Mech., vol. 35, pp. 89–111, 2003.

[6] Goldstein, Herbert (1980), Classical Mechanics (2nd ed.), Reading, MA: Addison-Wesley, ISBN 978-0-201-02918-5

[7] Klumpp, A. R., Singularity-Free Extraction of a Quaternion from a Direction-Cosine Matrix, Journal of Spacecraft and Rockets, vol. 13, Dec. 1976, p. 754, 755.

[8] G. Rodriguez, A. Jain and K. Kreutz-Delgado, Spatial operator algebra for manipulator modeling and control, Int. J. Robot. Res. 10(4) (1991), 371–381.

[9] J.J. Bernstein and M.S. Weinberg. 5 March 1996. U.S. Patent #5,496,436, "Comb-Drive Micromechanical Tuning Fork Gyro Fabrication Method."

[10] Kalman, R.E. (1960). "A new approach to linear filtering and prediction problems". Journal of Basic Engineering 82 (1): 35–45. Retrieved on 2008-05-03.

[11] Iyer, B.R.; Vishveshwara, C.V. (1993), "Frenet-Serret description of gyroscopic precession", Phys. Rev., D 48 (12): 5706–5720.